Analysis and Design of a High-Performance Bi-directional PWM Converter for DC Bus and Battery Bank Interface

Luciano Schuch, Cassiano Rech, Humberto Pinheiro, Hélio Leães Hey,
Hilton Abílio Gründling and José Renes Pinheiro
Power Electronics and Control Research Group – GEPOC
Federal University of Santa Maria – UFSM
CEP: 97015-900 – Santa Maria, RS – Brazil
lschuch@sm.conex.com.br, renes@ctlab.ufsm.br - http://www.ufsm.br/gepoc/

***Abstract* – This paper presents in depth analysis and design of a bi-directional PWM converter (buck/boost) used to interface as a critical dc bus and a battery bank. A detailed design procedure for the power and control circuit is proposed. With this design procedure, the definition of the operation frequency of each converter takes into account the different power and voltage levels at loads in order to reduce the commutation losses without degrading the specifications imposed to the converter. Furthermore, it is proposed the utilization of an appropriate filter to minimize the current and voltage ripples at battery, leading to an increased battery life without penalizing the volume and/or the switching frequency of the converter. Experimental results based on a 580 W prototype are presented to validate the proposed design procedure and to demonstrate the performance of the proposed approach. Additionally, a boost preregulator was included at input stage for power factor correction.**

I. INTRODUCTION

Nowadays, the electric power supply quality has become an indispensable factor for low power systems. Thereby, the demanding market of uninterruptible power systems (UPS) has been increasing. This increase in the demand requires the development of high efficiency, low cost and compact systems. In uninterruptible power systems, the cost of the batteries has a major impact in the overall system cost [1]. The choice flexibility of the battery bank voltage level makes possible to reduce the number of batteries that compose it for a desired autonomy, reducing the cost of battery bank. With this, it is usually necessary the adaptation of the battery bank voltage level for that required by critical load (dc bus).

The life and capacity of the battery depend on several factors, such as: charge and discharge mode, maintenance, temperature and age. Among these factors, the charge and discharge mode presents the greatest influence in the life and capacity of the battery [2]. The choice of the most appropriate charge method depends mainly on the battery type and its application. For the Valve Regulated Lead Acid batteries (VRLA), the most appropriate method is the one current level and one voltage level method (UI) [3], [4]. Furthermore, the battery bank must be recharged with current and voltage with low ripple levels, as in high frequency (switching frequency) as in low frequency (AC utility frequency and its multiples). In this manner, the converters connected to the battery must satisfy these requests.

In [5] and [6] are presented battery chargers which have been designed to reduce the converter losses, their weight and volume. However, these converters present charge current with significant low frequency ripple (120 Hz), which decreases the battery life. On the other hand, in [7] a battery charger with no low frequency current ripple is presented. Nevertheless, the volume and/or the switching frequency of the converters are elevated when a high frequency small ripple is desired.

This paper proposes a design procedure of the power devices and the control of bi-directional (buck/boost) PWM (Pulse Width Modulation) converter used for dc bus and battery bank interface. The definition of the operation frequency of each converter takes into account the different power and voltage levels at loads in order to reduce the commutation losses without degrading the specifications imposed to the converter. Furthermore, it is proposed the utilization of an appropriate filter to minimize the current and voltage ripples at battery, leading to an increased battery life without penalizing the volume and/or the switching frequency of the converter. In this way, the proposed approach can minimize the disadvantages previously mentioned. In addition, in the attempt to meet standard recommendations (like IEC 1000-3-2), a preregulator converter was included at input stage as shown in Fig. 1.

This paper is organized as follows. Section II describes the converter in study. Design procedure of the bi-directional converter is proposed in Section III. Section IV presents a design example and Section V shows a description of the converter control approach. Finally, Section VI presents the experimental results obtained for a 580 W prototype.

II. CONVERTER DESCRIPTION

In Fig. 2 is shown the bi-directional converter considered for an application in which the primary source come from the rectification of the AC utility. Moreover, it is necessary to adjust the voltage level of the dc bus by a boost converter.

The input boost converter (preregulator) is composed by a bridge rectifier, an inductor (L_{bb}), a diode (D_3), a switch (S_3) and a capacitor (C_b). An input filter (C_{fin} and L_{fin}) was included to the preregulator, as presented in Fig. 2, to minimize the input current distortion and the electromagnetic interference (EMI).

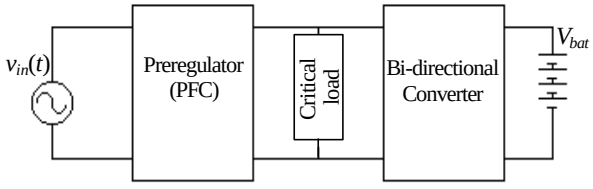

Fig. 1. Power stages of the studied converter.

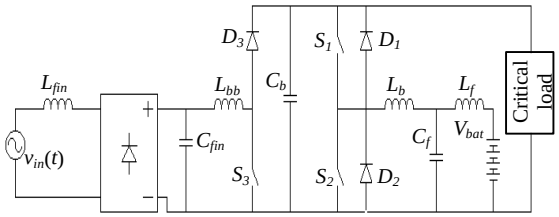

Fig. 2. Studied converter.

Additionally, the bi-directional converter (buck/boost) has two main switches (S_1 and S_2), two main diodes (D_1 and D_2), one battery bank and one T filter composed by two inductors (L_b and L_f) and one capacitor C_f. This converter is part of a stand-by system, which has the function of charge the battery bank and to supply energy to the load in the AC utility falls. The operation of the bi-directional converter depends on the state of the utility. In Fig. 3(b) is shown that if the AC utility operates normally, the switch S_1 is operating to charge the battery bank and in Fig. 3(c) is depicted that when AC utility falls the switch S_2 will be operating to supply energy to the load. Therefore, this converter operates in two different ways and alternately, one as a buck converter (S_1-D_2) and the other as a boost converter (S_2-D_1).

III. Design Procedure of the Bi-Directional Converter

The challenge of the design procedure of the power devices is in the fact that the bi-directional converter operates either buck or boost. These two operation states are different because they process different power and current levels. Thus, the switches S_1 and S_2 and the diodes D_1 and D_2 do not present the same specifications. Therefore, the design of the converter must consider that the switch S_1 and diode D_2 process low power (80 W) and S_2 and D_1 process a high power (500 W). Therefore, to have an appropriate cost-benefit relationship between the commutation losses and the volume/weight of the converter, the switching frequency must be correctly determined. The converter of greater power (with large current levels) operates with lower frequency and the converter of lower power (with lower current levels) operates at higher frequency. With this, through an appropriate design procedure, the commutation losses are reduced without altering the specifications imposed to the converter.

The specifications to design the bi-directional converter are:

P_0 = Output power (W)
V_0 = Output voltage (V)
V_{bat} = Battery bank voltage (V)
$\Re_1$ = Current ripple during the battery charge (%)
$\Re_2$ = Current ripple in the L_b inductor (%)
I_{bat} = Battery charge current (A)

Firstly, it is performed the design of the inductor L_b and of the operation frequency of the switch S_2 in function of the battery discharge (boost mode). At last, it is performed the design of the inductor L_f, capacitor C_f and of the operation frequency of the switch S_1 in function of the battery charge, when power transfer occurs from input source to the batteries (buck mode).

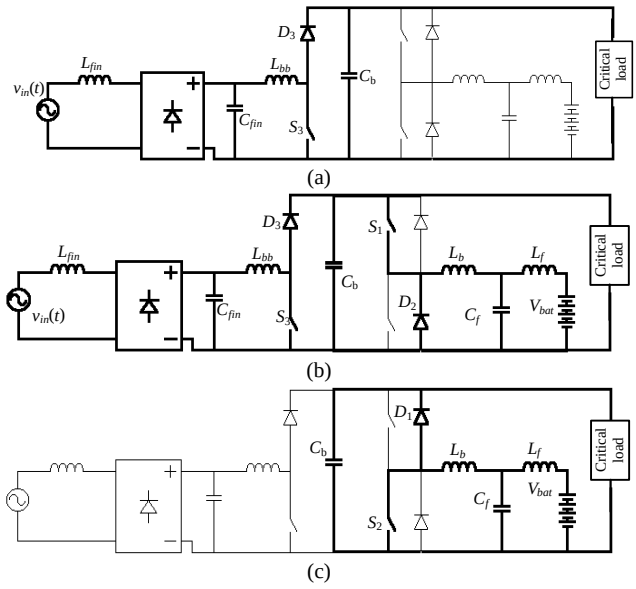

Fig. 3. Operation states of the converter in study: (a) Input boost (preregulator); (b) Buck; (c) Output boost.

A. Boost Converter

Initially, the operation frequency of the switch S_2 must be defined. So, the value of the inductance L_b is given by:

$$L_b = \frac{V_{bat}^{\,2}(V_o - V_{bat})10^2}{\Re_2 V_0 P_0 f_{s2}} \quad (1)$$

B. Buck Converter

The value of the inductance L_f is calculated from the relationship shown in inequality (2) and the cutoff frequency of the T filter is defined as at least ten times smaller than the operation frequency of the switch S_2, as shown bellow:

$$50 \le \frac{L_b}{L_f} \le 150 \quad (2)$$

$$fc_T \le \frac{f_{s2}}{10} \quad (3)$$

Inequality (2) should be attended for the filter T do not affect the power transfer of the output boost converter.

From the values of L_f, L_b and fc_T the value of the capacitor C_f is given by:

$$C_f = \frac{L_b + L_f}{4p^2 fc_T^2 L_f L_b} \quad (4)$$

To determinate the operation frequency of the switch S_1, it is used the abacus shown in Fig. 4 (Section IV), which relates the charge current ripple of the battery and the operation frequency of the switch S_1.

IV. Design Example

The design specifications of the bi-directional converter are shown in Table I.

Table I– Design specifications.

Output power (W)	P_0 = 500 W
Output voltage (V)	V_0 = 360 V
Battery bank voltage (V)	V_{bat} = 48 V
Current ripple during the battery charge (%)	$\hat{A}_1$ = 0.2 %
Inductor current ripple L_b (%)	$\hat{A}_2$ = 40 %
Switching frequency S_2	f_{s2} = 40 kHz
Battery charge current (A).	I_{bat} = 1.4 A

The results have been obtained by using four batteries of the model UNIKOR 12V7AH. To guarantee an appropriate charge time and an extended battery life, the charge current must be approximately equal to 1.4 A [4].

The choice of the frequency f_{s2} takes into account the cost-benefit relationship between the commutation losses and boost diode reverse-recovery related losses, and the volume/weight of the converter. As shown in Fig. 5, the frequency f_{S2} was defined as 40kHz because at this point occurs the intersection of the curve A_exA_w with the line of the P_s+P_{rr} losses.

Fig. 5 was obtained from (5), (6) and (7), varying the output boost switching frequency from 1kHz to 200kHz.

$$A_e xA_w = \frac{V_{Lb}\, I_{Lbrms} 10^4}{f_s\, K_w B_{\max} J_{\max}} \tag{5}$$

$$P_s = \frac{1}{2} V_0\, I_{Lb}\; fs(t_{c(on)} + t_{c(off)}) \tag{6}$$

$$P_{rr} = V_0\, f_s I_{rr}\left(\frac{3t_a + 2t_b}{6}\right) \tag{7}$$

Where: A_e is the effective cross-sectional area, A_w available window area, K_w factor of use of the area of the winding, B_{max} maximum flux density, J_{max} maximum current density in the contuctor of the inductor, P_s average power loss, $t_{c(on)}$ turn-on crossover interval, $t_{c(off)}$ turn-off crossover interval, P_{rr} reverse-recovery loss of the boost diode, t_a and t_b are subperiods of turn-on time and I_{rr} peak reverse-recovery current value of the boost diode.

From the specifications presented in Table I, it can be obtained the value of L_b from the equation (1):

$$L_b = 249.6mF\ .$$

Defining that the inductance L_f is 150 times smaller than the inductance L_b (to obtain an inductor of small volume), and using (3) and (4), the values of L_f, f_{cT} and C_f are:

$$L_f = 1.67\ \mu\text{F},$$
$$fc_T = 4kHz\ ,$$
$$C_f = 1mF\ .$$

By using the abacus shown in Fig. 4 and defining that the battery current ripple should be equal to 0.2 % of battery charge current, the operation frequency of the switch S_1 corresponds to approximately:

$$f_{s1} \cong 97kHz\ .$$

This abacus was obtained from (8), varying the buck switching frequency from 10kHz to 300kHz.

$$i_{ripple}(\%) = \left(\frac{i_{Lfpico} - i_{Lf}(0)}{i_{Lf}(0)}\right)100 \tag{8}$$

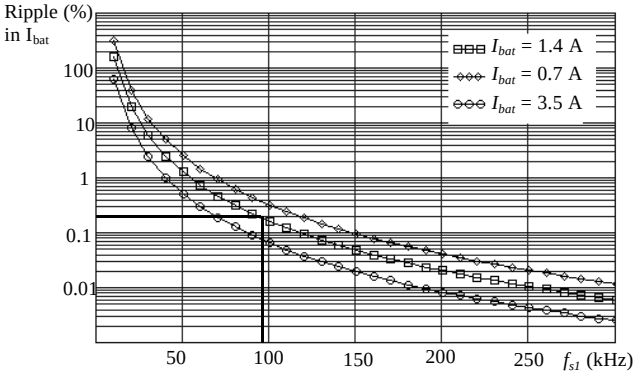

Fig. 4. Ripple of the battery current *x* S_1 frequency.

V. Converter Control

The charge of the battery bank (buck converter) can present two operation modes: voltage mode (float mode) and current mode. Block diagrams of these two systems are shown in Fig. 6 and Fig. 7, respectively, where the proportional control has been used for the voltage mode and the average current mode control [8] has been used for the current mode.

To obtain the mathematical model of the buck converter in the voltage and current modes, the battery bank was substituted by an equivalent circuit shown in Fig. 8, based on the battery model presented in [9]. The R_s value is obtained directly from the battery datasheet, and the R and C values are obtained from the constant time RC, which is calculated from the battery bank charge time.

In Fig. 6, $C_1(s)$ is the proportional controller, $G_1(s)$ is the plant and $H_1(s)$ is the sensor gain.

The proportional controller $C_1(s)$ and the transfer function $G_1(s)$ are given by:

$$C_1 = K_p\ , \tag{9}$$

$$G_1(s) = V_i \frac{B_0 s^2 + B_1 s + B_2}{A_0 s^4 + A_1 s^3 + A_2 s^3 + A_3 s + A_4}\ , \tag{10}$$

where

$$A_0 = L_f C_f L_b R\, C, \tag{11}$$
$$A_1 = C_f L_f L_b + C_f L_b R_s R\, C, \tag{12}$$
$$A_2 = C_f L_b R + C_f L_b R_s + L_b R\, C + L_f C\, R, \tag{13}$$
$$A_3 = R_s R\, C + L_b + L_f, \tag{14}$$
$$A_4 = R + R_s, \tag{15}$$
$$B_0 = L_f C\, R\ , \tag{16}$$
$$B_1 = L_f + R_s R\, C, \tag{17}$$

and

$$B_2 = R + R_s. \tag{18}$$

The compensator design has been made by using (19), based on the final value theorem.

$$K_p \geq V_s \frac{V_{fref} - \Delta V_f H}{\Delta V_f H^2 Vi\min} \tag{19}$$

Then, defining that the error of the float voltage must be smaller than 1%, the K_p value is:

$$K_p \geq 22$$

In Fig. 7, $H_e(s)$ represents the switching effect [10], $G_2(s)$ is the plant, $H_2(s)$ is the sensor gain and $C_2(s)$ is the current compensator. These transfer functions are given by:

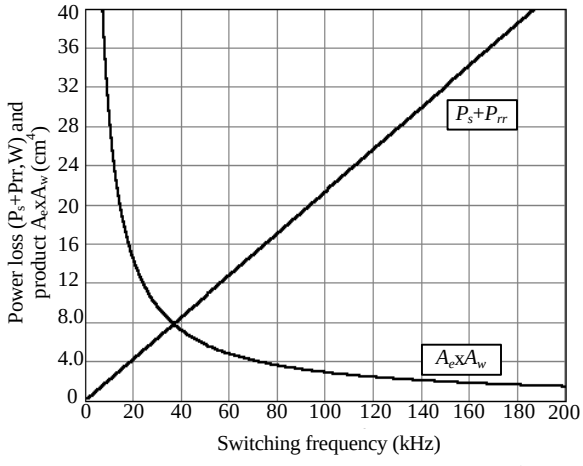

Fig. 5. Average power loss (P_s+P_{rr}) and product A_exA_w *x* S_2 frequency.

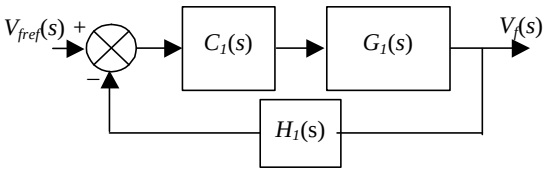

Fig. 6. Block diagrams of the system in voltage mode.

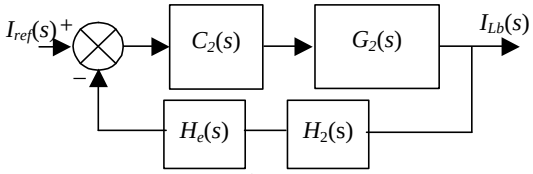

Fig. 7. Block diagram of the system in current mode.

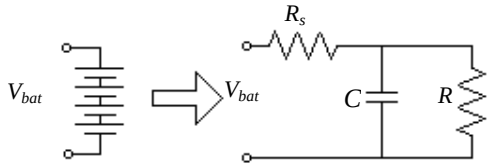

Fig. 8. Equivalent circuit of the battery bank.

$$H_e(s) = \frac{s^2}{(p.f_{s1})^2} - \frac{s}{2.f_{s1}} + 1 \tag{20}$$

$$G_2(s) = V_i \frac{RCs+1}{L_b RC s^2 + (R_s RC + L_b)s + (R+R_s)} \tag{21}$$

$$C_2(s) = \frac{K_c\left(1+\frac{s}{w_z}\right)}{s\left(1+\frac{s}{w_p}\right)} \tag{22}$$

where

$$K_c = \frac{1}{R_l\left(C_{fp}+C_{fz}\right)}, \tag{23}$$

$$w_p = \frac{C_{fz}+C_{fp}}{R_f C_{fz} C_{fp}}, \tag{24}$$

and

$$w_z = \frac{1}{R_f C_{fz}}. \tag{25}$$

The current compensator can be designed as follows. The high-frequency pole, w_p, should be placed near the switching frequency in order to provide sufficient filtering for switching frequency ripple. After, the zero, w_z, should be placed at half of cutoff frequency of the output filter to maximize current loop crossover frequency. Finally, the compensator gain is given by:

$$\frac{R_f}{R_l} \le \frac{2V_s L f_s}{(V_i - V_o)K_k} \tag{26}$$

The compensator output may intersect the ramp signal again in the off-time period if the dc gain is higher than that defined by (26), leading to switching stability [8].

With this, the current compensator parameters w_p, w_z and K_c, for the proposed topology, are given by:

w_p= 628320 rad/s, w_z = 12566 rad/s and K_c =4300.

The output voltage control is realized by the voltage loop of the output boost converter, Fig. 9, or by the voltage loop of the preregulator converter, Fig. 10.

In Fig. 9, $C_3(s)$ is a proportional-integral (PI) compensator, $G_3(s)$ is the plant and $H_3(s)$ is the sensor gain. These transfer functions are given by:

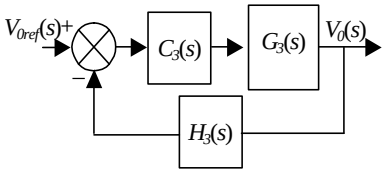

Fig. 9. Block diagram of the output boost.

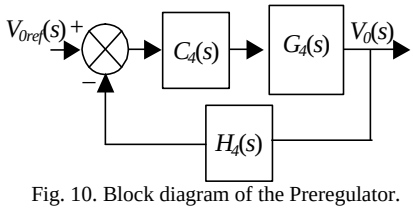

Fig. 10. Block diagram of the Preregulator.

$$C_3 = K_{PI}\frac{(s+z_{PI})}{s} \tag{27}$$

$$G_3(s) = A\frac{-\frac{L_{eq}}{R_0}s + \left(1-\frac{R_{eq}}{R_0}\right)}{L_{eq}C_b s^2 + \left(\frac{L_{eq}}{R_0}+R_{eq}C_b\right)s + \left(1-\frac{R_{eq}}{R_0}\right)} \tag{28}$$

where

$$A = \frac{V_{bat}R_0}{(R_{eq}+R_0)\bar{d}^2}, \tag{29}$$

$$L_{eq} = \frac{L_b}{\bar{d}^2}, \tag{30}$$

$$R_{eq} = \frac{R_s}{\bar{d}^2}, \tag{31}$$

and

$$\bar{d} = \frac{V_{bat}}{V_0}. \tag{32}$$

The voltage compensator of the output boost converter can be designed as follows. The zero, z_{PI}, should be placed at most one fifth before the lower frequency pole of the plant and the gain, K_{PI}, is calculated so that the bandwidth of the closed-loop system is three times greater than the bandwidth of the original system. In this way, the compensated system has a good dynamic response. Thus, for the proposed topology, the K_{PI} and z_{PI} parameters are:

K_{PI} = 5 and z_{PI} = 34.4 rad/s.

In Fig. 10 $G_4(s)$ is the plant, $C_4(s)$ is a PI compensator and $H_4(s)$ is the sensor gain. These transfer functions are given by:

$$G_4(s) = V_{in}\frac{\sqrt{\frac{2R_0.T}{L_{bb}}\left(1-\frac{V_{in}}{V_0}\right)}}{\left(1-\frac{V_{in}}{V_0}\right)C_b R_0 s + \left(2-\frac{V_{in}}{V_0}\right)} \tag{33}$$

$$C_4 = K_{PI}\frac{(s+z_{PI})}{s} \tag{34}$$

The PI compensator of the preregulator converter can be designed by using the following equations:

$$z_{PI} = \frac{2-\frac{V_{in}}{V_0}}{\left(1-\frac{V_{in}}{V_0}\right)R_0 C_b} \tag{35}$$

$$K_{PI} = \frac{w_{cc} V_s \sqrt{w_{cc}^{\ 2} + z_{PI}^{\ 2}}}{\sqrt{w_{cc}^{\ 2} + z_{PI}^{\ 2}} G H} \quad (36)$$

where

$$w_{cc} = 2p\ f_{cc} \quad (37)$$

and

$$G = V_i \frac{\sqrt{L_{bb} R_0 T \left(1 - \frac{V_{in}}{V_0}\right)}}{\left(1 - \frac{V_{in}}{V_0}\right) R_0 C_b} \quad (38)$$

The crossover frequency, f_{cc}, used to design the PI compensator is 12 Hz. Any increase in the crossover frequency would increase the input current distortion and, consequently, would decrease the input power factor. Thus, the K_{PI} and z_{PI} values are given by:

K_{PI} = 3.126 and z_{PI} = 14.844 rad/s.

VI. Experimental Results

A prototype of the proposed converter has been built in laboratory, using the parameters obtained in the design example, for the verification of the design procedure. In Table II are presented the parameters of the implemented prototype.

Table II– Parameters of the implemented prototype

Input AC voltage	V_{in} =110 ± 20 % V_{rms} f = 60 Hz
Output voltage	V_0 = 360 V
Battery bank voltage	V_{bat} = 48 V
Prergulator power	P_p =580 W (P_0 + P_{bat})
Output power	P_0 = 500 W (R_0 = 259.2 Ω)
Input filter	C_{fin} = 5 µF L_{fin} = 375 µH
Buck frequency	f_{s1} = 100 kHz
Boost frequency	f_{s2} = 40 kHz
Preregulator frequency	f_{s3} = 20 kHz
T filter	C_f = 1 mF L_f = 1,6 µH L_b = 250 µH
Boost capacitor	C_b = 680 µF
Boost inductor (preregulator)	L_{bb} = 166 µH

In Fig. 11 are shown the input voltage and input current waveforms, presenting a power factor equal to 0.99 and in Fig. 12 is presented the output voltage waveform.

The proposed system shown in Fig. 1 is classified as a class D equipment by the standard IEC 1000-3-2. This standard establishes the maximum limits of low order current harmonics (3rd to 19th for class D equipments).

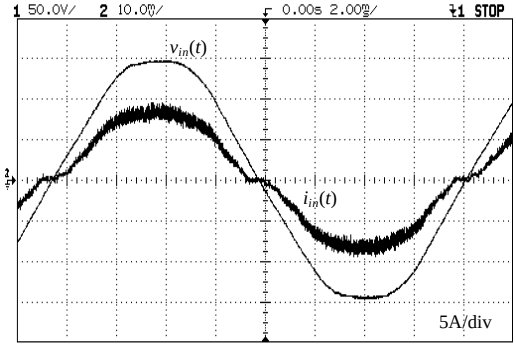

Fig. 11. Input voltage and input current of the preregulator converter (50V/div., 5A/div., 2ms/div.).

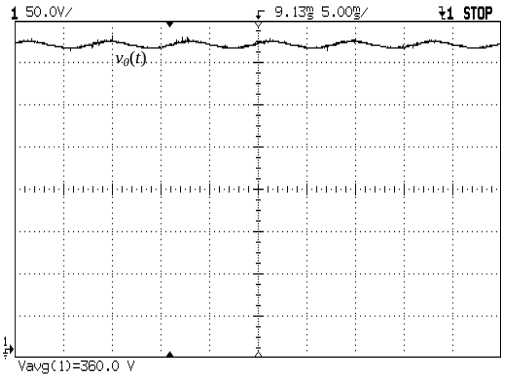

Fig. 12.: Output voltage of the preregulator converter (50V/div., 5ms/div.).

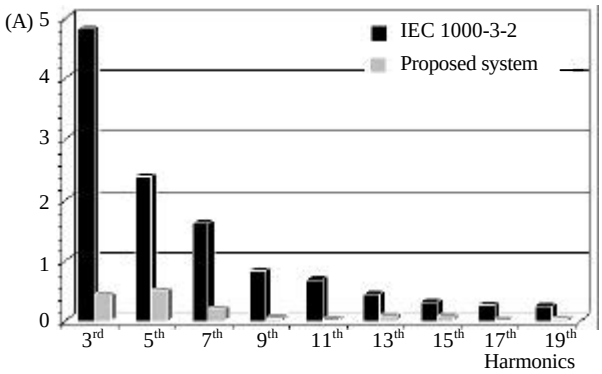

Fig. 13. Comparison between the current harmonics injected into the public supply system by the converter with the limits specified by the IEC 1000-3-2.

Fig. 13 presents a comparison between the current harmonics injected into the public supply system by the converter with the limits specified by the IEC 1000-3-2.

In Fig. 14 and in Fig. 15 are shows the main waveforms when the bi-directional converter is operating as a boost converter, that is, when AC utility falls. In Fig. 14 are presented the current waveforms in the inductors L_b and L_f, proving that the current drained from battery bank presents low ripple. Fig. 15 shows the output voltage and battery bank voltage waveforms.

In Fig. 16 and in Fig. 17 are presented the main waveforms when the bi-directional converter is operating as a buck converter. Fig. 16 shows the current waveforms through the inductor L_b and the batteries (current mode), confirming that the battery is charged with a current with low ripple levels. In addition, Fig. 17 presents the battery bank voltage waveform in the voltage mode.

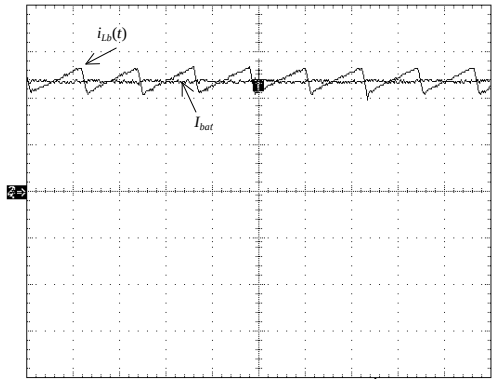

Fig. 14. Current in the inductors L_b and L_f of the output boost converter (5A/div., 20µs/div.)

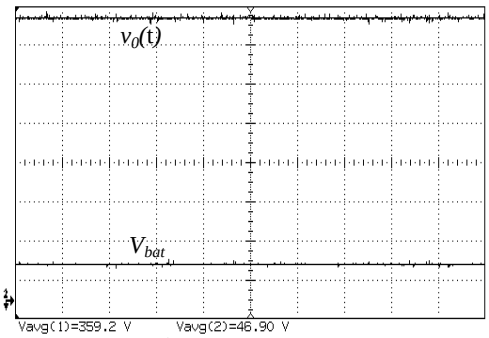

Fig. 15.. Output voltage of the output boost converter and battery bank voltage (50V/div, 5ms/div).

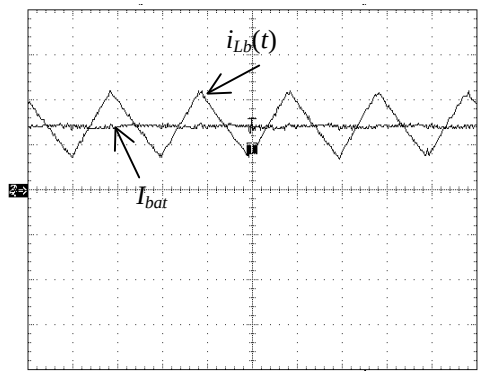

Fig. 16. Buck converter in current mode: current in L_b and I_{bat} (1A/div. and 5μs/div.).

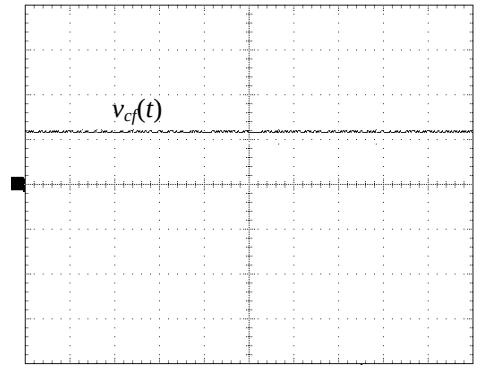

Fig. 17. Buck converter in voltage mode: float voltage (50V/div. and 5ms/div.).

Efficiency, THD and power factor of the proposed topology in function of the output power are presented in Fig. 18, where it is possible to verify that the efficiency, the THD and the power factor are, respectively, 91.4%, 12% and 0.99, for full-load.

VI. CONCLUSIONS

The bi-directional converter used in this paper can be easily adapted to operate in several uninterruptible power systems. By using the proposed design procedure, the bi-directional converter can guarantee the specifications without penalizing the volume of the converter. With appropriate choice of the switching frequencies of the switches S_1 e S_2, in which the switch of large power operates with lower frequency and vice-versa, it is obtained a reduction of commutation losses of the converter.

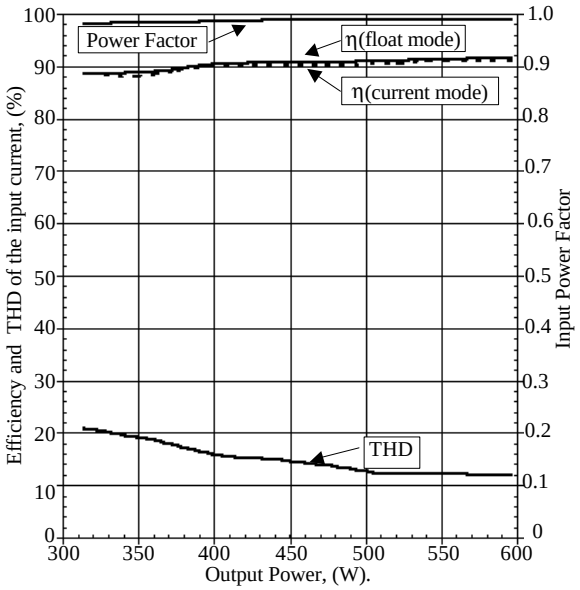

Fig. 18. Efficiency, input current THD and power factor of the proposed topology (V_{in} = 110V_{rms}, V_0 = 360V e V_{bat} = 55V).

Other important characteristic of the bi-directional converter is that the choice flexibility of the voltage level of the battery bank makes possible to reduce the number of batteries that compose it for a desired autonomy, reducing the cost of battery bank.

Moreover, using the proposed T filter and an appropriate charge method (IU), the battery bank is charged and discharged with low high frequency current and voltage ripple and without low frequency (120Hz) ripple, maximizing the lifetime and the capacity of the batteries. It has been experimentally demonstrated the good performance of the proposed approach for a 580 W prototype.

REFERENCES

[1] B. Essig, G. Braun, “Selecting Batteries for Uninterruptible Power Supply Systems”, in *IEEE APEC Conference Proceedings*, 1991, pp. 642-645.

[2] D. G. Vutetakis, H. Wu, “The effect of Charge Rate and Depth of Discharge on the Cycle Life of Sealed Lead-Acid Aircraft Batteries”, in *IEEE 35th International Power Sources Symposium*, 1992, pp. 103-105.

[3] T. Suntio, “A Novel Method to Ensure Full Recharge of a VRLA Battery String”, in *IEEE INTELEC Record*, 2000, pp. 755-760.

[4] W. Fischer, Stationary Lead-Acid Batteries An Introductory Hand Book, Germany, Hoppecke batterien, 1994.

[5] P. Bartholomeus, M. Le, “Battery Charger with High Quality Input Waveforms”, in *ISIE Record*, 1995, pp. 574-579.

[6] I. Barbi, E. V. Kassick, “A Low Cost High Power Factor Resonant Mode Battery Charger”, in *IEEE APEC Conference Proceedings*, 1993, pp. 543-548.

[7] J. A. O’Connor, “Simple Switchmode Lead-Acid Battery Charger”, *Unitrode Application Note*, 1995-96, pp. 10-260 – 10-268.

[8] J. Sum, R. M. Bass, “Modeling and Practical Design Issues for Average Current Control” in *IEEE APEC Conference Proceedings*, 1999, pp. 980-986.

[9] Z. M. Salamch, M. A. Casacca, W. A. Lynch, “A Mathematical Model for Lead-Acid Batteries” in *IEEE Trans. on Energy Conversion*, vol. 7, no 1, pp. 93-97, march 1992.

[10] R. B. Ridley, “A New, Continuous-Time Model For Current-Mode Control” in IEEE Transactions on Power Eletronics, vol. 6, no 2, pp. 271-278, april 1991.

[11] International Electrotechnical Commission, “ICE 1000-3-2: Electromagnetic Compatibility (EMC) – Part 3: Limits – Section 2: Limits for Harmonic Current Emissions”, 1995.